# CHAPTER IV
# NICKEL LOADED ALUMINA VIA SOL-GEL PROCESS

## 4.1 Abstract

Supporting nickel has been used in a wide range of applications for industrial reactions, such as, steam reforming, hydrogenation and methanation. In this work, nickel aluminate was prepared by sol-gel process using alumatrane as alkoxide precursor, directly synthesized from the reaction of inexpensive and available compounds, aluminium hydroxide and TIS (triisopropanolamine) via the Oxide One Pot Synthesis (OOPS) process. Various conditions of the sol-gel process, viz. pH, calcination temperature, hydrolysis ratio and ratio of nickel to aluminum are studied. All samples are characterized using FTIR, TGA, XRD, TPR, DR-UV and BET. The BET surface area measurements are found to be in the range of 300-450 $m^2/g$ at the calcinations temperature of 500°C having the pore distribution in the mesoporous region. The catalyst activity tasting on CO oxidation reaction depends on Ni to Al ratio and calcinations temperature. The higher activity was obtained from the higher Ni content and lower calcination temperature. In addition, catalysts prepared using alumatrane precursor had higher % conversion than those prepared from aluminium hydroxide.

**KEYWORDS:** Sol-gel Process, Alumatrane, Nickel aluminate

## 4.2 Introduction

The uses of supported metal oxide catalysts are applicably important, especially to most of petrochemical industries due to their wide range applications of industrially important reactions. Several studies on alumina-supporting nickel catalyst [1-2] revealed the formation of nickel aluminate spinel, $NiAl_2O_4$, being a stable compound with strong resistance to acids, alkalis, and having high melting

point and surface area. More importantly, nickel aluminate is capable of resistance to deactivation by coke formation [3].

Traditionally dried mixing of ceramics and metal powders followed by heat treatment is often difficult to control, resulting in non-uniform dispersion of the components. In contrast to chemical technique, sol-gel process offers several advantages. It is low cost and allows greater control in size and morphology. It can design materials of specifically macroscopic morphology, such as ultra-fine particle, fiber, thin film and monolith. The sol-gel process is one of the most interesting ways to prepare nickel aluminate. This process is performed at low temperature followed by appropriate heat treatment. It provides a uniform microstructure with a high degree of dispersion between the metal and ceramic phases [4]. In addition, this process gives high product purity. Owing to the hydrolysis reaction involved, water can induce so called "sol", subsequently condensed to metal oxide network, leading to a gel formation. Parameters in the sol-gel process, such as, pH, proportion of water used for the hydrolysis and the presence of either acid or base catalyst [5], are important. In addition, calcinations temperature and duration of calcination also have a significant impact on the final structure and texture of nickel aluminate spinel. An increase in calcinations temperature results in a development of crytallization of $NiAl_2O_4$ [3].

Generally, the metal alkoxides, such as, aluminium *sec*-butoxide, aluminium isopropoxide, are popular metal oxides used as ceramic precursors due to the purity of starting materials and the low temperature for a reaction to occur. However, there are also disadvantages from these metal alkoxides, which are expensiveness and low hydrolytic stability. These problems have been resolved by synthesis of simple alkoxide precursors containing one or more alkoxide ligands, making them more hydrolytic stability because of the obstruction of coordination site at the metal. The function of chelating agent is to retard the hydrolysis and condensation reaction rates in order to obtain homogeneous gels. Aluminium hydroxide can be used as a precursor, but the gelation of aluminium hydroxide occurs rapidly. It is thus difficult to obtain a uniform gels. This problem can be solved by slowing down the precursor's reactivity by either using a strong mineral acid [6] or using a chelating,

such as, triisopropanolamine or TIS to form alumatrane complexes [7] to be used as a precursor for preparing high surface area alumina [5].

In this work, alumatrane is used as an alkoxide precursor for loading nickel onto alumina by means of the sol-gel process. Optimal conditions to obtain high surface area and the catalyst activity test on CO oxidation reaction of nickel aluminate are investigated.

## 4.3 Experimental

### *Materials*

Aluminium hydroxide hydrate [$Al(OH)_3$ $xH_2O$] was purchased from Sigma Chemical Co. Triisopropanolamine (TIS, $N(CH_2CHCH_3OH)_3$) and nickel acetate [$(CH_3COO)_2Ni$] were obtained from Aldrich Chemical Co. Inc.(USA). They were used as a received. Ethylene glycol (EG, $HOCH_2CH_2OH$) used as solvent for the alumatrane synthesis was purchased from J.T. Baker Inc. (Phillipburg,USA). Acetronitrile ($CH_3CN$) and methanol were obtained from Lab-Scan Company Co., Ltd. and distilled before use. Nitric acid and ammonia solution used to adjust pH in the sol-gel process were purchased from Lab-Scan Company Co., Ltd., and used as received.

### *Equipment*

Functional groups of materials were followed using FTIR spectrophotometer (Nicolet, NEXUS 670) with a resolution of 4 $cm^{-1}$. The solid samples were mixed and pelletized with dried KBr. Thermogravimetric analysis (TGA) was carried out using TG-DTA (Pyris Diamond Perkin Elmer) with a heating rate of 10°C/min in the range of room temperature to 750°C under nitrogen atmosphere to determine the thermal stability of alumatrane. Powder X-ray diffraction (XRD) patterns were carried out to characterize crystallinity of samples using a Rigaku X-ray diffractometer with CuKα as a source. A range from 5° to 90° was investigated using a step of 5°/min. The diffuse reflectance UV-VIS spectra were collected on a SHIMADZU UV 2550-VISIBLE spectrophotometer in the range of 190 to 900 nm.

The reducibility was investigated by temperature-programmed reduction on TPD/R/O/MS Themo Finnigan 1100. The reducing gas is 5% $H_2$ in $N_2$ at a flow rate of 40 ml/min. The rate of temperature was carried out at the heating rate of 10°C/min ranging from room temperature up to 900°C. The BET surface area measurement, pore volume and pore size distribution were measured by using nitrogen at 77 K in Autusorb-1 gas sorption system (Quantasorb JR). Samples were degassed at 250°C under a reduced pressure prior to each measurement. The morphology was studied on SEM using JEOL 5200-2AE scanning electron microscope.

## Methodology

### *Synthesis of alumatrane by the OOPS process*

The preparation of alumatrane or tris(alumatranyloxy-*i*-propyl)amine was followed Wongkasemjit *et al*'s works [5,7] via the Oxide One Pot Synthesis (OOPS) process. Aluminium hydroxide, TIS and EG are added into a 250 ml two-necked round bottom flask. The mixture was homogeneously stirred at room temperature before being heated to 200°C under nitrogen in an oil bath for 10 h. Excess EG was removed under vacuum ($10^{-2}$ Torr) at 110°C to obtain crude product. The crude solid was washed with acetonitrile and dried under vacuum at room temperature. Dried products were characterized using TGA and FTIR.

### *Nickel loading onto alumina using alumatrane precursor via the sol-gel process*

Alumatrane was used as an alumina source via the sol-gel process at various Ni/Al ratios, pH, hydrolysis ratios and calcinations temperature. Alumatrane and nickel acetate were dissolved in methanol for 1 h before adding water and adjusting pH. The pH value of the unadjusted mixture solution is pH 9. For acid conditions, pH 3, 5 and 7, $HNO_3$ was used whereas $NH_4OH$ was added for obtaining pH 11. Three hydrolysis ratios of 9, 18, 27, as followed the previous work [5], were investigated. The solution was vigorously stirred at room temperature followed by heat treatment of the resulting gels at calcinations temperature ranging from 500°C to 900°C and held at the final temperature for 7 h.

*Activity testing on CO oxidation reaction*

The catalytic tests of CO oxidation with $O_2$ were carried out in a fixed-bed flow reactor in the temperatures ranging from 200°-450°C. A 0.2 g of catalyst was employed for each experiment. For the reaction condition, 180 ml/min total gas flow was maintained with feeding the reaction mixture of CO-$O_2$-He (1%-2%-97%).

## 4.4 Results and Discussion

*Synthesis of alumatrane precursor*

Alumatrane precursor was synthesized from aluminium hydroxide and TIS via the Oxide One Pot Synthesis (OOPS) process. The product obtained was a white solid. The structure of alumatrane showing in Fig.1 contains trialkanoamine ligand which results in hydrolytic stable, as mentioned earlier. The function of this chelating agent is to slow down the rates of hydrolysis and condensation reactions to obtain homogeneous gels during the sol-gel process.

The TGA result of alumatrane (Fig. 2) showed two major transitions of weight loss. The first region between 50°-250°C indicated the decomposition of solvent trapped in the product and TIS ligand while the second region at about 250°-500°C corresponded to the decomposition of the organic ligands and carbon residues. The % ceramic yield of the product was 33 % which was higher than the theoretical ceramic yield (23.7 %) due to the incomplete combustion of the product which can be confirmed by the darker ash obtained.

FTIR spectrum of the alumatrane precursor is shown in Fig. 3 The broad band at 3300-3700 $cm^{-1}$ is the characteristic of O-H stretching vibration. The peak at 2725-3000 $cm^{-1}$ corresponds to the stretching vibration of C-H bond. The peak position at 1650 $cm^{-1}$ is assigned to the O-H overtone. The peak position at 1450 $cm^{-1}$ is the bending vibration of C-H bond. The peak position at 1000-1200 $cm^{-1}$ is resulted from the C-N and/or O-H stretching vibrations. The peaks at 1078 and 500-800 $cm^{-1}$ indicate the stretching vibration of Al-O-C and Al-O of alumatrane, respectively.

***Nickel loading onto alumina via the sol-gel process***

The preparation conditions and calcinations temperatures have significant impact on the final structure and texture of nickel loaded alumina. XRD patterns of nickel-alumina samples showed poor crystallinity at low calcinations temperatures (Fig. 4). As increasing calcinations temperature, crystallization of samples can be developed further. Calcinations at increasing temperature were also accompanied by color changes of the catalysts from greenish to light blue coloration. However, due to the overlaps of the XRD peaks of $Al_2O_3$ and $NiAl_2O_4$ phases, the 2θ values and the relative intensities were used to identify characteristics of the samples. The major peaks of the $NiAl_2O_4$ are the 2θ values at 37 (I=100%) and 45 (I=60-65%), whereas the major peaks of $Al_2O_3$ are the 2θ values at 37 (I=80%) and 45 (I=100%). The results of XRD patterns correspond to the three major peaks at 37(100), 45(65) and 65.5(60) of the nickel aluminate (ASTM#10-339) phase. The crystallinity of $NiAl_2O_4$-like spinel phase improves slightly with the increase of the Ni/Al ratio, as shown in Fig. 5. At lower Ni/Al ratio, the spinel phase is a solid mixture of $NiAl_2O_4$ and $Al_2O_3$. The $NiAl_2O_4$ phase improves when increasing the Ni/Al ratio (using the intensity ratio of the 2θ values at 37 and 45 degrees as indicators)

Effects of pH and hydrolysis ratio in Fig. 6 and 7, respectively, do not show any significant difference for the samples calcined at 500°C. Moreover, the results from the effect of hydrolysis ratio of the samples calcined at 900°C in Fig. 8 show the same pattern. However, the samples prepared at pH 3 in Fig. 9 show lower intensity than other pHs of the samples calcined at 900°C due to too much acid added into the system, causing faster the hydrolysis reaction rate, than the condensation reaction rate. All the samples from these XRD results are an indication of the formation of nickel aluminate, showing no formation of a nickel oxide-like phase.

FTIR analysis of the samples (Fig. 10) calcined at various calcinations temperature shows two bands at 3000-3700 and 1300-1700 $cm^{-1}$ corresponding to the stretching and bending vibrations, respectively, of the O-H bonds of water contained in the samples. The IR bands observed below 1000 $cm^{-1}$ can be attributed to the stretching vibrations of M-OH modes (M = Ni, Al). The FTIR spectra at lower calcinations temperature showing the broad band at 600 $cm^{-1}$ is the characteristic of

the $NiAl_2O_4$ structure [4]. $NiAl_2O_4$ spinel is clearly identified in the sample calcined at 800° and 900°C, showing the bands at 730, 600 and 500 $cm^{-1}$. These bands are related to the M atoms presenting both octahedral and tetrahedral sites. The FTIR spectra of $NiAl_2O_4$ at various hydrolysis ratios after calcination of 900°C in Fig. 11 show the same pattern. Fig. 12 shows the FTIR spectra of the samples calcined at 900°C and different pHs. There is no significant difference, except that the pH at 3 showed the lower intensity than others. This is in agreement with the XRD results. The higher intensity of the band below 1000 $cm^{-1}$ was obtained with increasing the ratio of Ni/Al, meaning that the higher Ni/Al ratio, the higher formation of nickel aluninate (Fig. 13).

Since crystallization of nickel aluminate is not well defined at low calcinations temperature, TPR was employed to investigate the reducibility of the catalysts and their corresponding nickel aluminate spinel. The TPR profiles (Fig. 14) of the catalysts calcined at 500°C show the maximum reduction temperature ($T_M$) at 600°C. The reduction temperature for this species is lower than bulk nickel aluminate spinel, but higher than NiO, indicating a strong interaction between nickel and alumina providing that the $NiAl_2O_4$ spinel was formed on the surface of the support [8]. The effect of calcinations temperature on the reduction profiles was also studied. The reduction profiles obtained for the samples calcined between 500°-900°C are shown in Fig. 14. Increase of calcinations temperature made the reduction increasingly more difficult as inferred from the shift of the main reduction peak and $T_M$ values to higher temperature. It is due to the larger crystallites sizes and the stronger interaction between metal and support as increasing calcinations temperature. This makes the reduction process more difficult. These results are coincided with those obtained by Cesteros *et al.* [2] and Pena *et al.* [3].

The influence of Ni loading on reducibility at various Ni/Al ratios, from the results in Fig. 15 showed that at lower Ni loading, the $T_M$ values were shifted to higher temperature due to a presence of relatively large proportion of unreduced nickel at low nickel containing catalysts which was stabilized at the vacancies of α-alumina with defective spinel structure [9]. It means that the reduction of Ni required higher temperatures as decreasing metal loading. The experiment condition and $T_M$

values obtained from the reduction profiles of supported Ni catalyst with various Ni loadings and calcinations temperature are given in Fig. 14 and 15. Both parameters had influence on the reducibility and the temperature of maximum reduction, which can be described as the interaction between metal and support.

The effects of pH and hydrolysis ratio as given in Fig. 16 and 17, the results showed the same reduction profiles which means that the reducibility of nickel aluminate prepared at various hydrolysis ratios and pHs were not significantly different.

To confirm the identity of nickel species and the formation of nickel aluminate, DR-UV analysis was conducted, as showed in Fig. 18-21. The characteristic bands in the region at 410 nm and around 600-645 nm are presented. In all samples a nickel aluminate spinel-like phase is formed. The bands at 410 and 600-645 nm indicate the distribution of the Ni(II) ions among octahedral and tetrahedral sites of alumina lattices like in a spinel structure, respectively [10]. The Ni(II) ions that enter in the $Al_2O_3$ lattices occupy simultaneously tetrahedral and octahedral sites in a ratio depended on the calcinations temperature. The higher calcination temperatures, the higher intensities of Ni(II) ions distributed in tetrahedral sites than the octahedral sites (Fig. 18). This is due to the fact that at the higher calcinations temperature the structure was collapsed, resulting in Ni ions to distribute more in tetrahedral sites of alumina than in octahedral sites because the hole in tetrahedral sites are smaller than that of octahedral sites. The samples calcined at 800° and 900°C occur the peak shifted, indicating that Ni ions distributed in octahedral sites of alumina from 410 nm to 375 nm due to the phase transformation of $\gamma$-$Al_2O_3$ to $\alpha$-$Al_2O_3$ [11]. In general, the $\alpha$-$Al_2O_3$ is usually found at the temperature exceeding 1200°C. However, the formation of the $\alpha$-$Al_2O_3$ phase can be formed at lower temperature which is the characteristic of the miscible oxide systems ($Co^{2+}$, $Ni^{2+}$, $Cu^{2+}$ and $Zn^{2+}$) [11]. NiO-$Al_2O_3$ calcined at 900°C was resulted from simultaneous crystallization of $NiAl_2O_4$ and $\alpha$-$Al_2O_3$ [11]. These results are corresponding to the results from XRD and FTIR.

In addition, when increasing the ratio of nickel to alumina, more Ni(II) ions diffused into alumina lattices at both octahedral and tetrahedral sites (Fig. 19). Except 4% Ni loading, the peak profile is different from others due to too small

amount of nickel aluminate formed and hardly detected by DR-UV. However, there is no significant difference at various pH and hydrolysis ratio of the samples prepared during the sol-gel process, as shown in Fig. 20 and 21.

Taking into account of these DR-UV studies, the structure of nickel spinel is partially inversed because of both octahedral and tetrahedral sites of Ni(II) ions distributing in the alumina lattices.

The BET surface areas determined are listed in Tables 1-4. It can be seen that for catalysts prepared in this work their specific surface areas are much larger than the results reported previously for the $Ni/Al_2O_3$ catalysts obtained from co-precipitaion method (S.A. 110-200 $m^2/g$) [2, 12] or from other precursors via the sol-gel process (S.A. 200-300 $m^2/g$) [1, 13] at the same calcinations temperature (500°C). All samples showed the pore size distribution in the mesoporous region having a pore diameter around 3-6 nm.

The effect of Ni/Al ratio resulted in the surface areas compared to blank alumina support (Table 1), indicating that the nickel metal was uniformly distributed in the final product [14]. It did not accumulate on the surface, but became integrated into the solid structure. The effect of calcinations temperature in Table 2 showed that the BET surface area of nickel aluminate decreased from 410 to 140 $m^2/g$ as the calcinations temperature increased from 500° to 900°C, whereas the crystallinity increased (sinterization). The BET surface area from samples prepared at various pHs in Table 3 showed the lower pH used, the lower surface area obtained because more amount catalyst added into the system made faster hydrolysis than condensation rates, not being able to form a perfect gel network. Thus, pH 9 which is the pH of isoelectric point of system [5] provided enough time to form a 3-D gel network giving the highest surface area. The effect of hydrolysis ratio as shown in Table 4 indicated that the samples prepared using the hydrolysis ratio of 18 showed the highest the BET surface area compared to other hydrolysis ratios. Low hydrolysis ratio leads to more difficult hydrolysis which consequently limits the condensation step. Thus, a higher water/alkoxide ratio would result in a great extent of hydrolysis and condensation reactions [15]. However, if too much water added during the sol-

gel process gives faster hydrolysis than condensation, resulting in weak branch and lower surface area.

SEM showed the morphologies of the samples calcined at 500°C in Fig. 22 a. The sample had rather amorphous with irregular shape. As increasing the calcinations to 700°C (Fig. 22 b), the morphology indicated higher crytallinity which is also in agreement with the XRD result.

The catalytic activity test on CO oxidation reaction with $O_2$ showed the temperature dependence on the conversion of CO oxidation reaction (Fig. 23). Their activities depend on the ratio of Ni to alumina. The activity increased with the increase of the Ni content.

Fig. 24 shows the activity results obtained from the samples calcined at different calcinations temperatures. Samples calcined at 500°C had higher % conversion than those calnined at 900°C due to the higher the BET surface area obtained at 500°C, providing better Ni ions distribution in lattices.

Further studies of the catalyst activities were carried out with different aluminium sources (Fig. 25). The samples synthesized from alumatrane precursor are more active than the samples produced by $Al(OH)_3$ precursor. This is probably due to the purer and more homogeneous nickel aluminate obtained from alumatrane precursor, giving better Ni ions distribution in alumina phase, while that obtained from aluminium hydroxide precursor contains a NiO phase in addition to a nickel aluminate phase.

## 4.5 Conclusions

Alumatrane synthesized from inexpensive and available compound via the one step process is successfully used as an alkoxide precursor for preparing nickel loaded alumina via the sol-gel route followed by heat treatment. The calcined samples favor the formation of nickel aluminate spinel, $NiAl_2O_4$, confirmed using XRD, FTIR, TPR and DR-UV. The calcinations temperature and the nickel content affected to the crytallinity of the samples. The higher crystallinity was resulted from the higher calcinations temperature and nickel content. A high Ni/Al ratio promotes

the inter-diffusion of Ni(II) ions into alumina phase, and the formation of tetrahedral sites as increasing the calcinations temperature. The BET surface area measurements are found to be in the range of 300-450 $m^2/g$ at the calcination temperature of 500°C, having the pore distribution in the mesoporous region. The activity testing on CO oxidation depends on Ni to Al ratio and calcinations temperature. The higher activity was obtained from the higher Ni content and lower calcinations temperature. Catalysts prepared using alumatrane precursor had higher % conversion than those prepared from aluminium hydroxide.

## 4.6 Acknowledgements

This research work is supported by the Postgraduate Education and Research Program in Petroleum and Petrochemical Technology (ADB) Fund, Ratchadapisake Sompote Fund, Chulalongkorn University, The Thailand Research Fund (TRF) and Development and Promotion of Science and Technology Thailand Project (DPST).

## 4.7 References

1. Arean,C.O., Mentruit,M.P., Lopez Lopez,A.J., Parra.J.B. (2001), High surface area nickel aluminate spinels prepared by a sol-gel method. Colliods and surfaces A:Physicochem.Eng.Aspects, 180, 253-258.
2. Cesteros,Y., Salagre,P., Medina,F., Sueiras,J.E. (2000), Synthesis and characterization of several $Ni/NiAl_2O_4$ catalysts active for the 1,2,4-trichlorobenzene hydrodechlorination. Applied catalysis B:Environmental, 25, 213-227.
3. Pena,J.A., Herguido,J., Guimon,C., Monzon,A., santamaria,J. (1996), Hydrogenationof Acetylene over $Ni/NiAl_2O_4$ Catalyst: Characterization, coking, reaction Studies. Journal of catalysis, 159, 313-322.

4. Rodeghiero,E.D., Moore,B.C., Wolkenberg,B.S., Wulthenow,M., Tse,O.K., Giannelis,E.P. (1998), Sol-gel synthesis of ceramic matrix composites. Material Sience and Engineering, A244, 11-21.
5. Ksapabutr,B., Gulari,E., Wongkasemjit.S. (2004), Sol-gel transition study and pyrolysis of alumina-based gels prepared from alumatrane precursor. Colloids and surfaces A:Physicochem.Eng.Aspects, 233, 145-153.
6. Suh,D.J., Park,T.J., Lee,S.H., Kim,K.L. (2001), Ni-alumina composite aerogels as liquid-phase hydrogenation catalysts. Journal of Non-Crystalline Solids, 285, 309-316.
7. Opornsawad,Y., Ksapabutr,B., Wongkasemjit,S., Laine,R.M. (2001), Formation and structure of tris(alumatranyloxy-*i*-propyl)amine directly from $Al(OH)_3$ and triisopropanolamine. European Polymer, 37, 1877-1885.
8. Xu,Z., Li,Y., Zhang,J., Chang,L., Zhou,R., Duan,Z. (2001), Bound-state Ni spices -a superior form in Ni-based catalyst for $CH_4/CO_2$ reforming. Applied Catalyst A: General, 210, 45-53.
9. Molina,R., Poncelet,G. (1998), α-Alumina-Supported Nickel Catalysts Prepared from Nickel Acetylacetonate:A TPR Study. Journal of catalysis, 173, 257-267.
10. Jitianu,M., Jitianu,A., Zahaarescu, M., Crisan,D., Marchidan,R. (2000), IR structural evidence of hydrotalcites derived oxidic forms. Vibratonal Spectroscopy, 22, 75-86.
11. Spivey,J.J., Agarwal,S.K. (1993). Catalysis Volume 10 : Applied of Raman Spectroscopy to Heterogeneous Catalysis. Royal Society of chemistry : London.
12. Chokkaram,S., Srinivasan,R., Milburn,D.R., Davis,B.H. (1997), Conversion of 2-octanol over nickel-alumina, cobalt-alumina, and alumia catalysts. Molecular Catalysis A: Chemical, 121, 157-169.
13. Piao,L., Li,Y., Chen,J., Lin,J.Y. (2002), Methane decomposition to carbon nanotubes and hydrogen on an alumina supported nickel aerogel catalyst. Catalyst today, 74, 145-155.
14. Suh,D.J., Park,T.J., Kim,J.H., Kim,K.L. (1998), Nickel-alumina aerogel catalysts prepared by fast sol-gel synthesis. Journal of Non-Crystalline Solids, 225, 168-172.

15. Pascual,E.R., Larrea,A., Monzon,A., Gonzalez,R.D. (2002), Thermal Stability of $Pt/Al_2O_3$ Catalysts Prepared by Sol-Gel. Journal of Solid State Chemistry, 168, 343-353.

## CAPTION OF TABLES AND FIGURES

**$Al(OH)_3$ + TIS + EG**

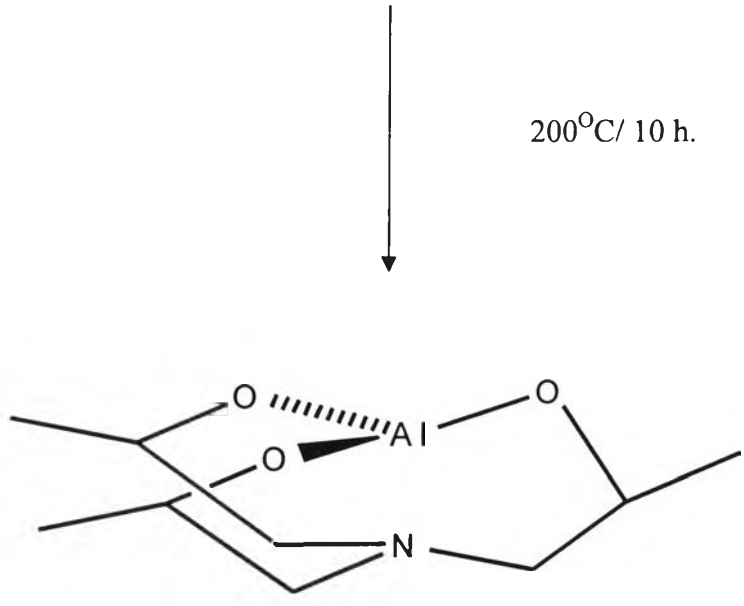


Figure 1.

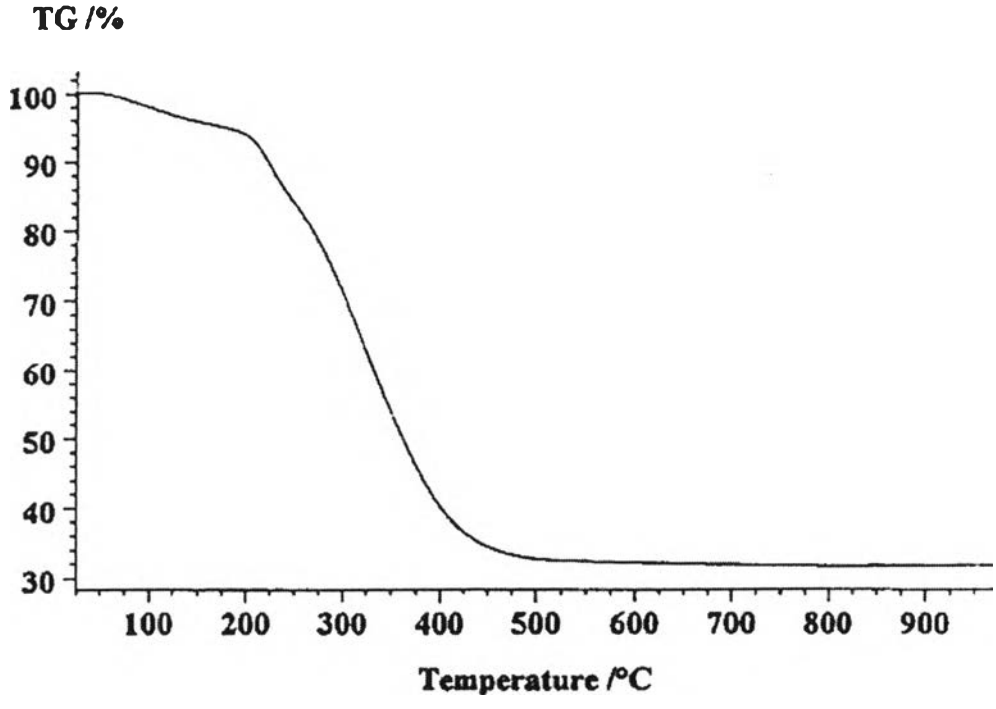
TG /%
100
90
80
70
60
50
40
30
100
200
300
400
500
600
700
800
900
Temperature /°C

Figure 2.

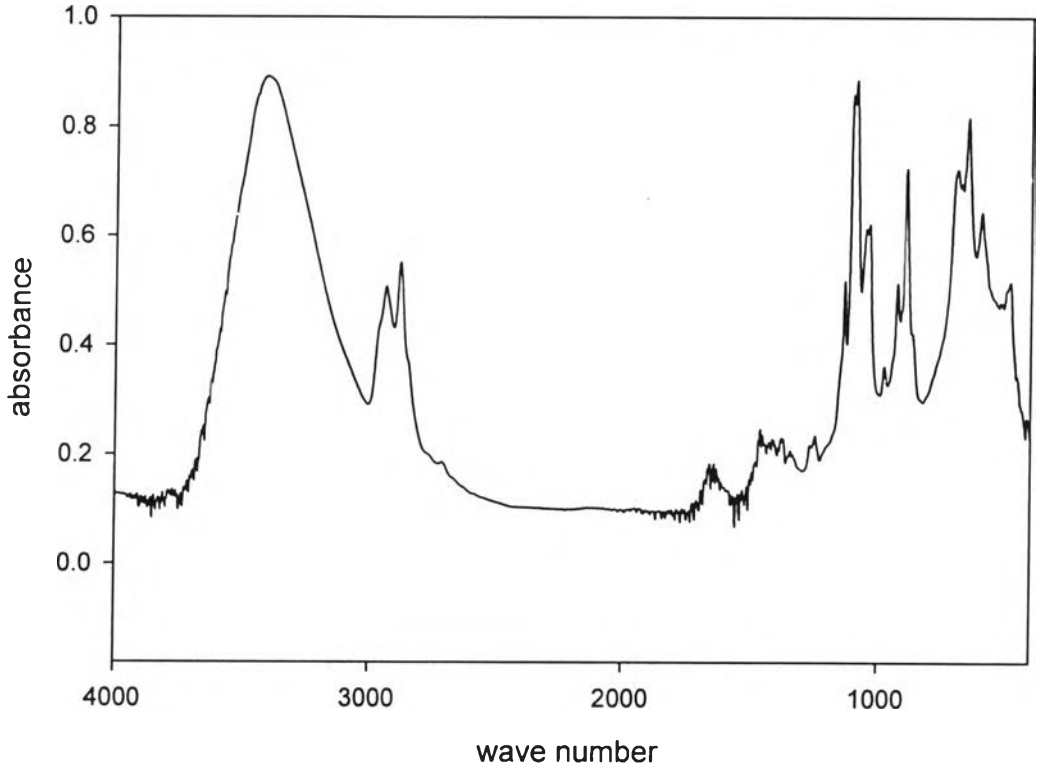


Figure. 3

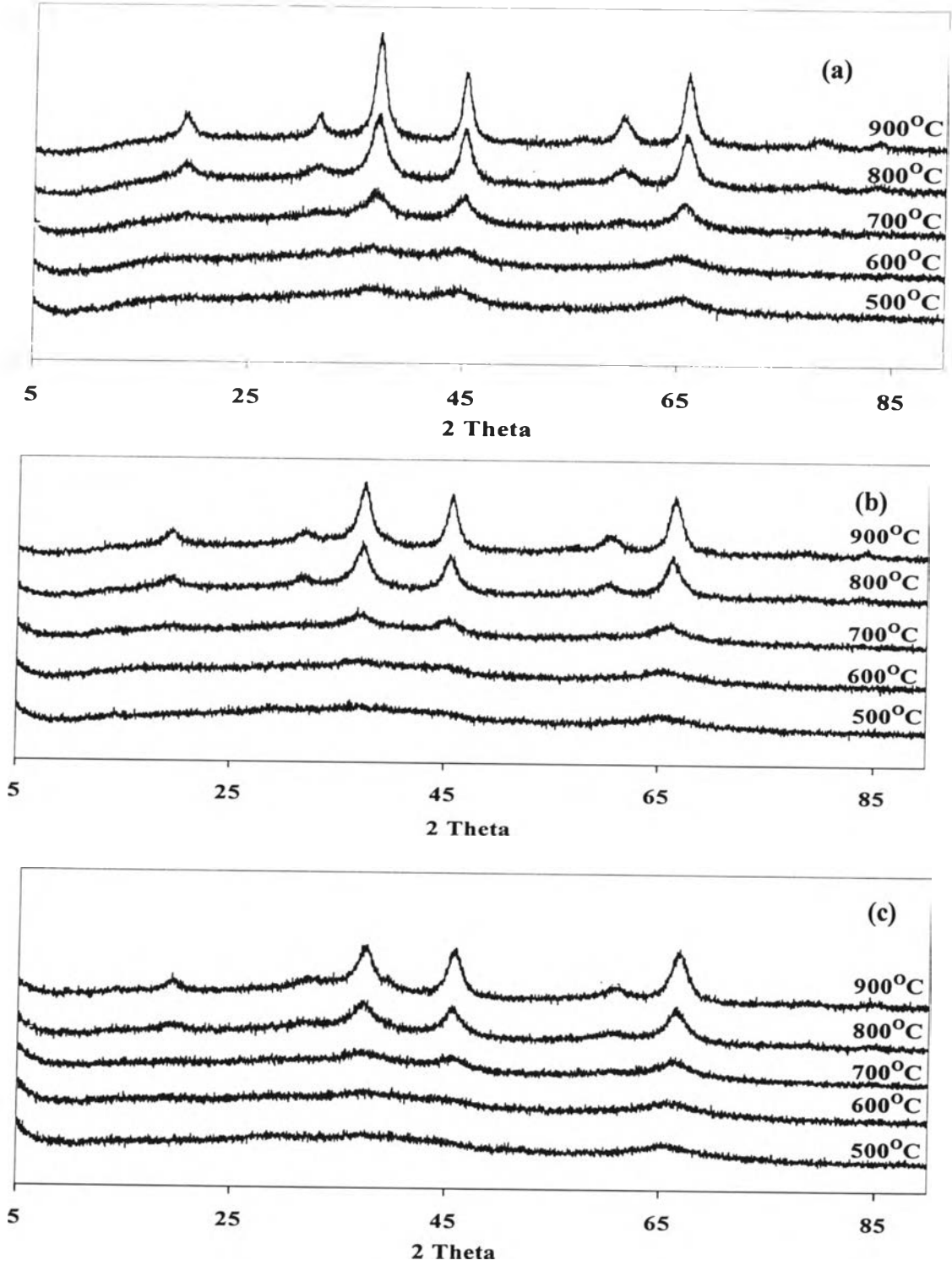
(a)
900°C
800°C
700°C
600°C
500°C
5
25
45
65
85
2 Theta
(b)
900°C
800°C
700°C
600°C
500°C
5
25
45
65
85
2 Theta
(c)
900°C
800°C
700°C
600°C
500°C
5
25
45
65
85
2 Theta

Figure 4.

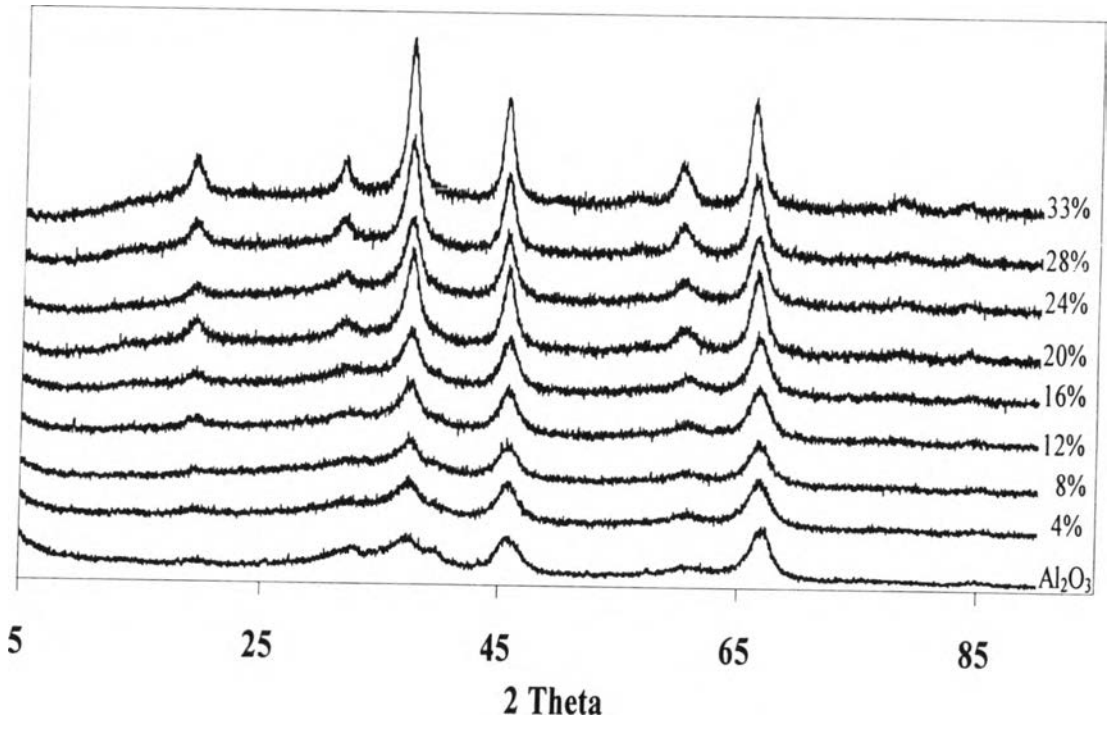


Figure 5.

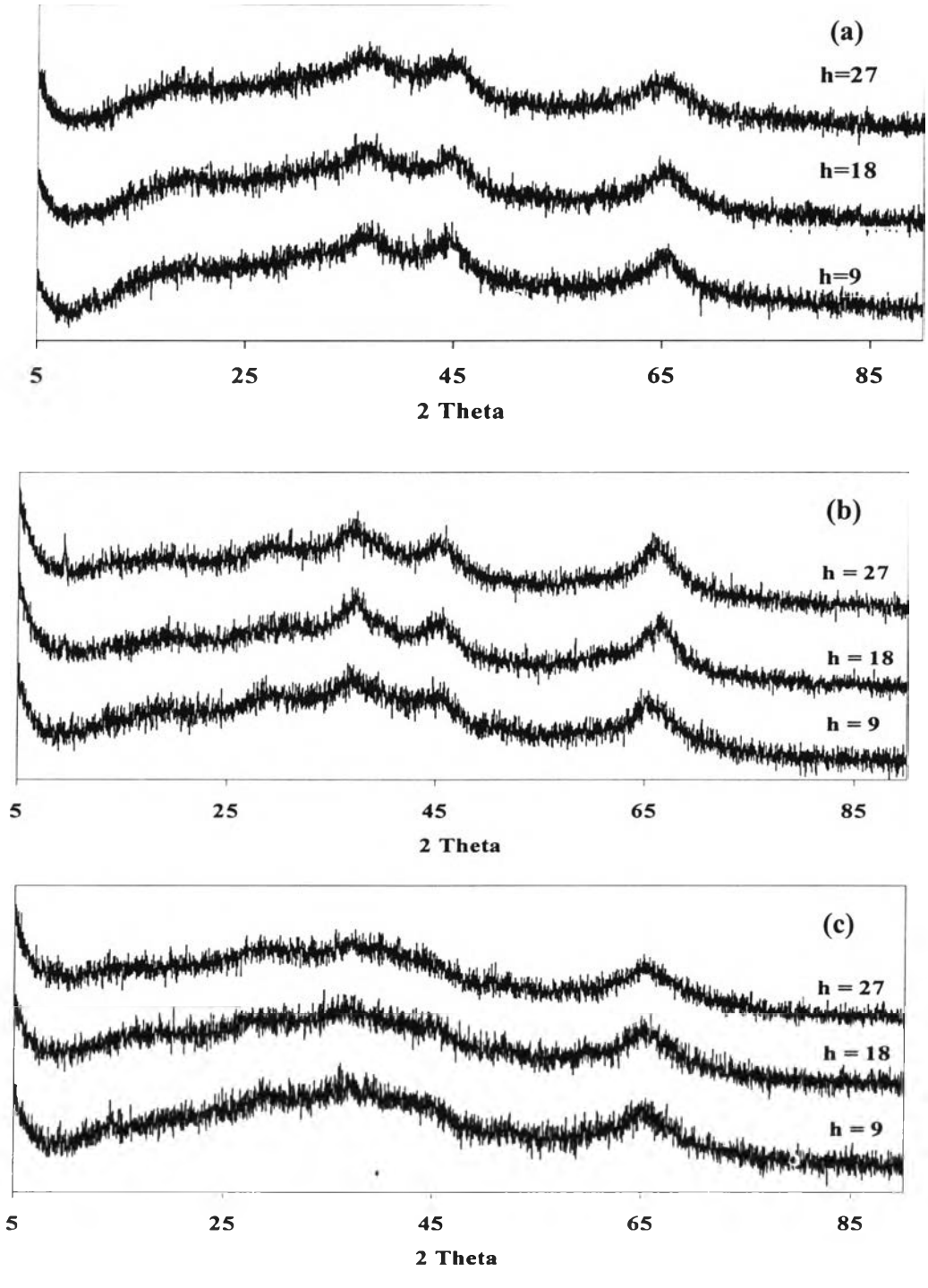
(a)
h=27
h=18
h=9
5
25
45
65
85
2 Theta
(b)
h = 27
h = 18
h = 9
5
25
45
65
85
2 Theta
(c)
h = 27
h = 18
h = 9
5
25
45
65
85
2 Theta

Figure 6.

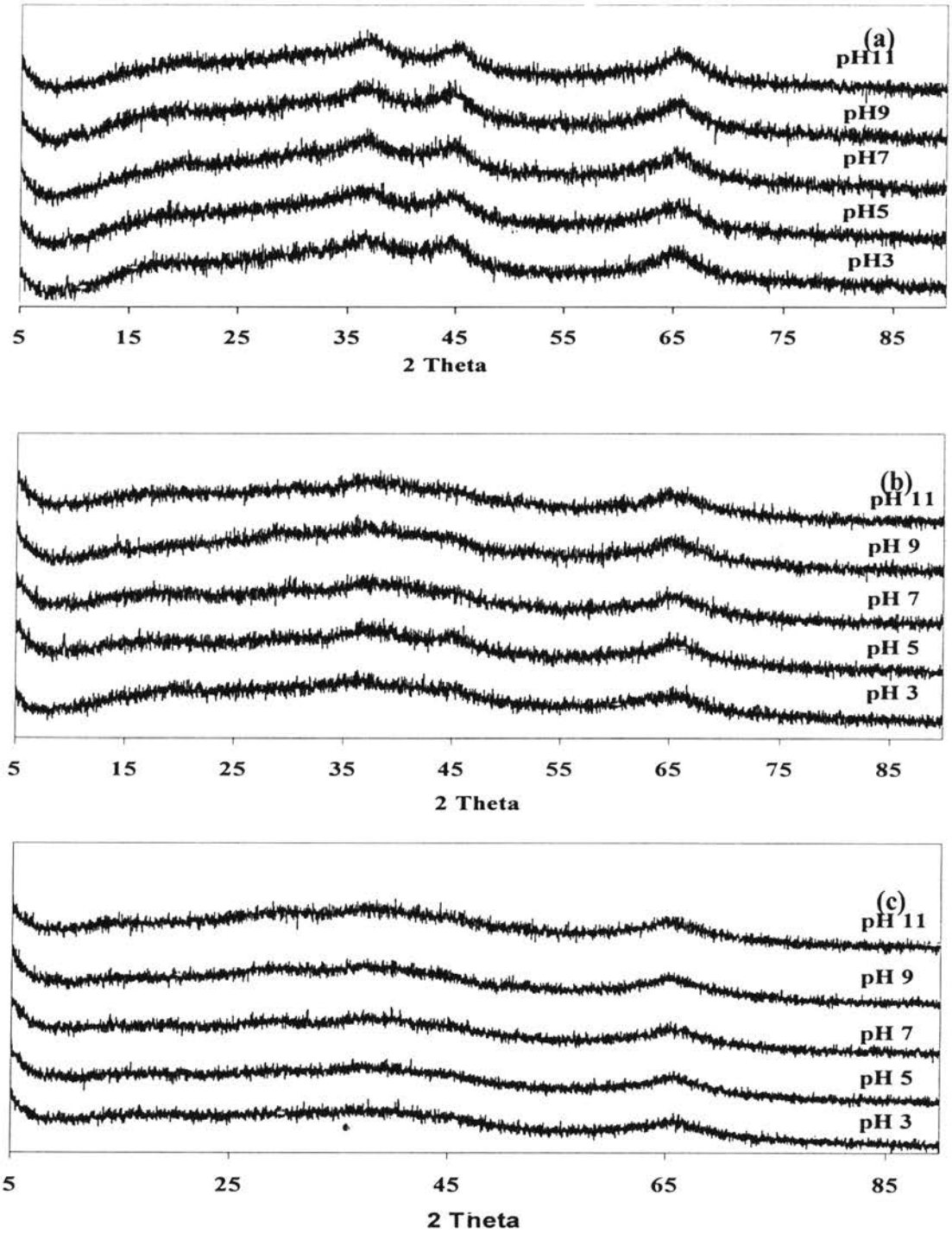
(a)
pH11
pH9
pH7
pH5
pH3
5
15
25
35
45
55
65
75
85
2 Theta
(b)
pH 11
pH 9
pH 7
pH 5
pH 3
5
15
25
35
45
55
65
75
85
2 Theta
(c)
pH 11
pH 9
pH 7
pH 5
pH 3
5
25
45
65
85
2 Theta

Figure 7.

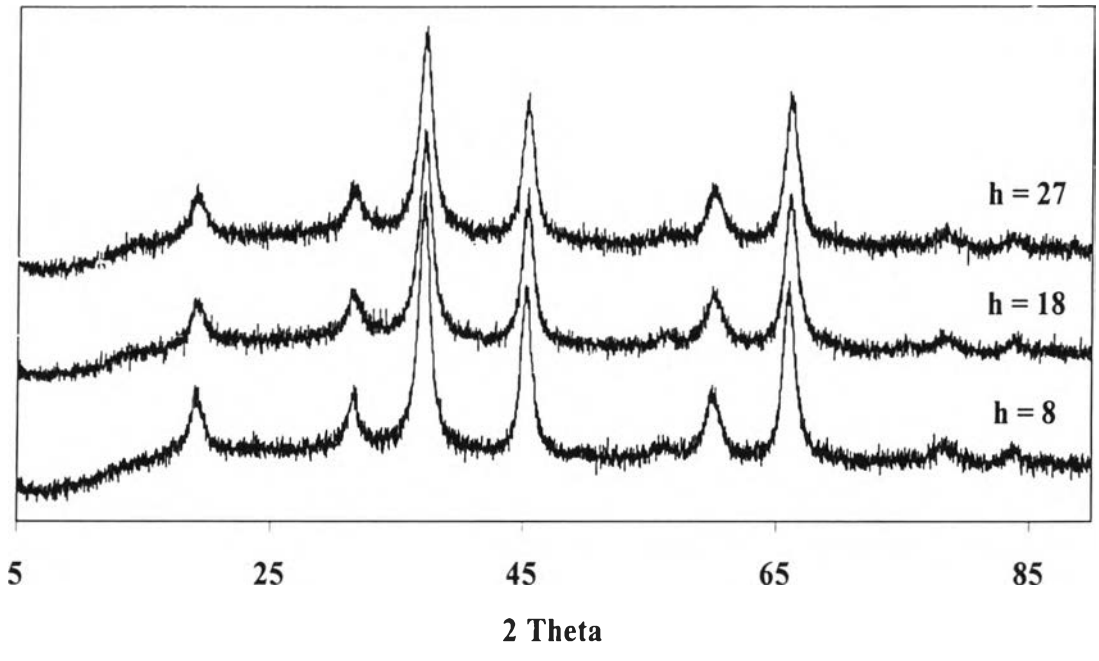


Figure 8.

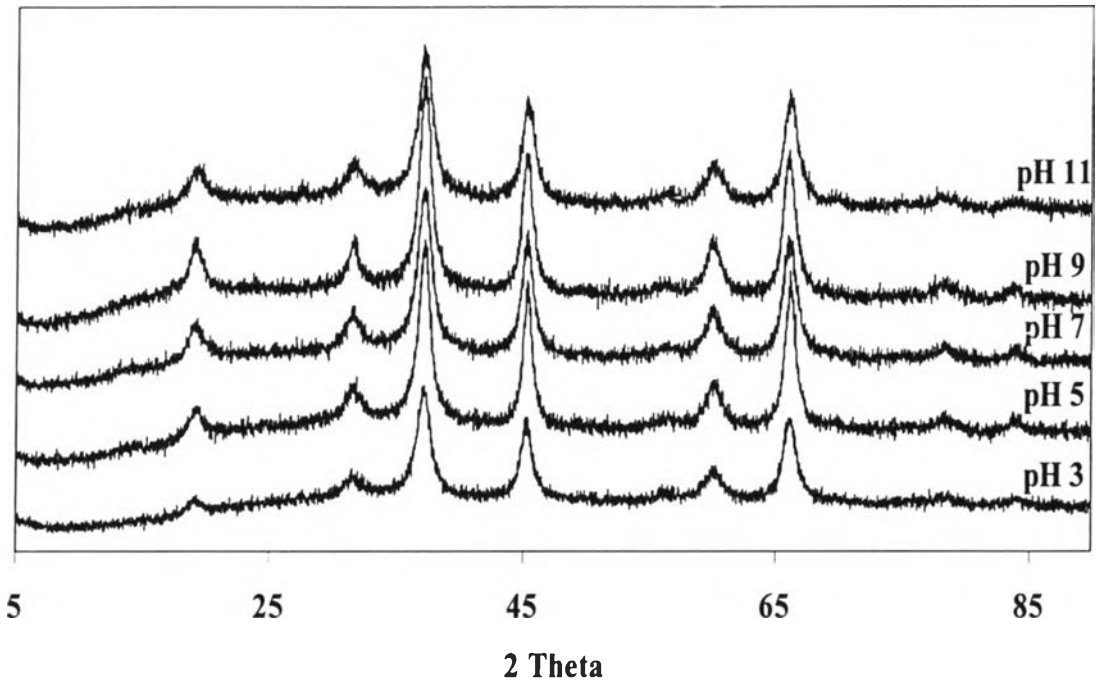


Figure 9.

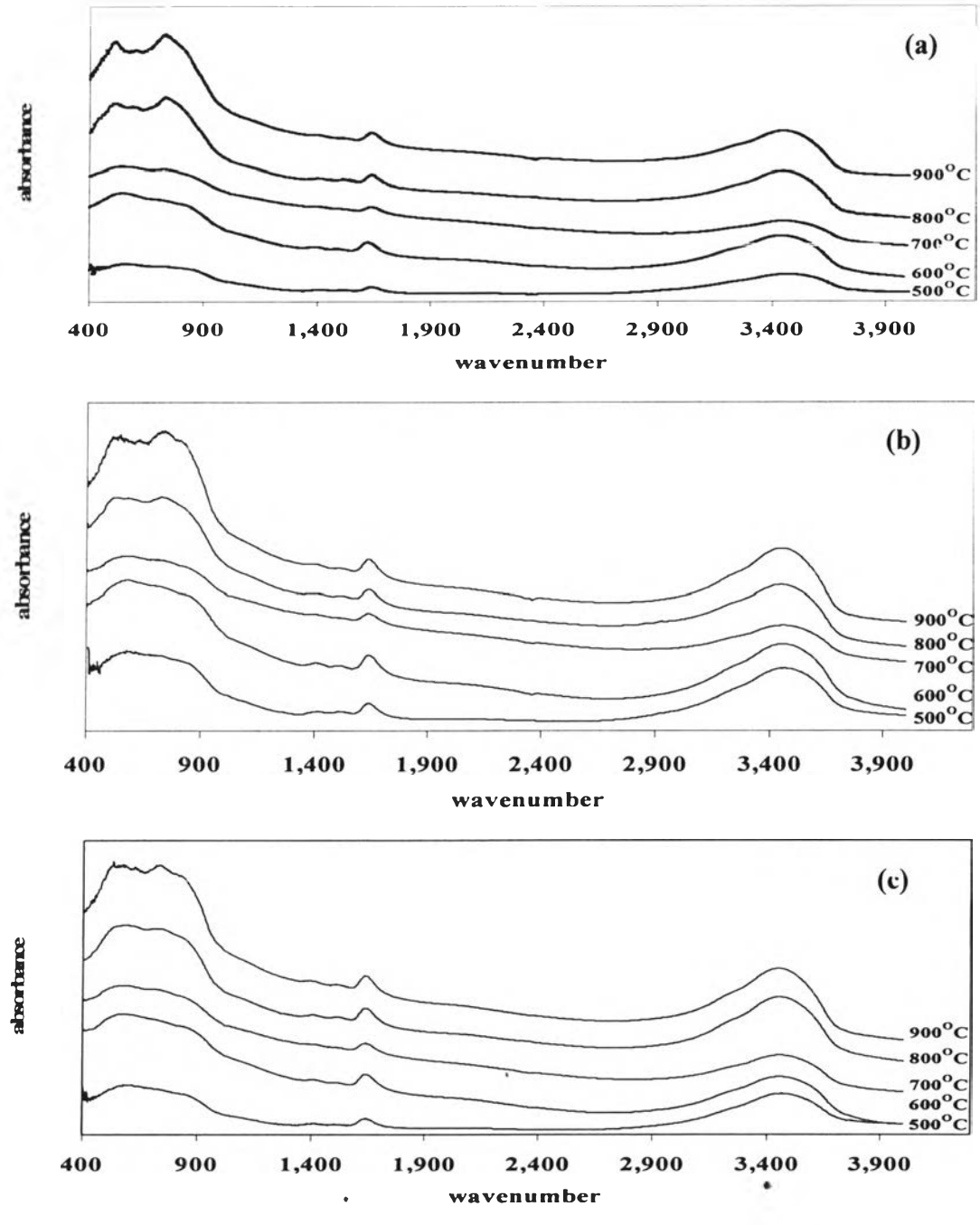
(a)
absorbance
900°C
800°C
700°C
600°C
500°C
400
900
1,400
1,900
2,400
2,900
3,400
3,900
wavenumber
(b)
absorbance
900°C
800°C
700°C
600°C
500°C
400
900
1,400
1,900
2,400
2,900
3,400
3,900
wavenumber
(c)
absorbance
900°C
800°C
700°C
600°C
500°C
400
900
1,400
1,900
2,400
2,900
3,400
3,900
wavenumber

Figure 10.

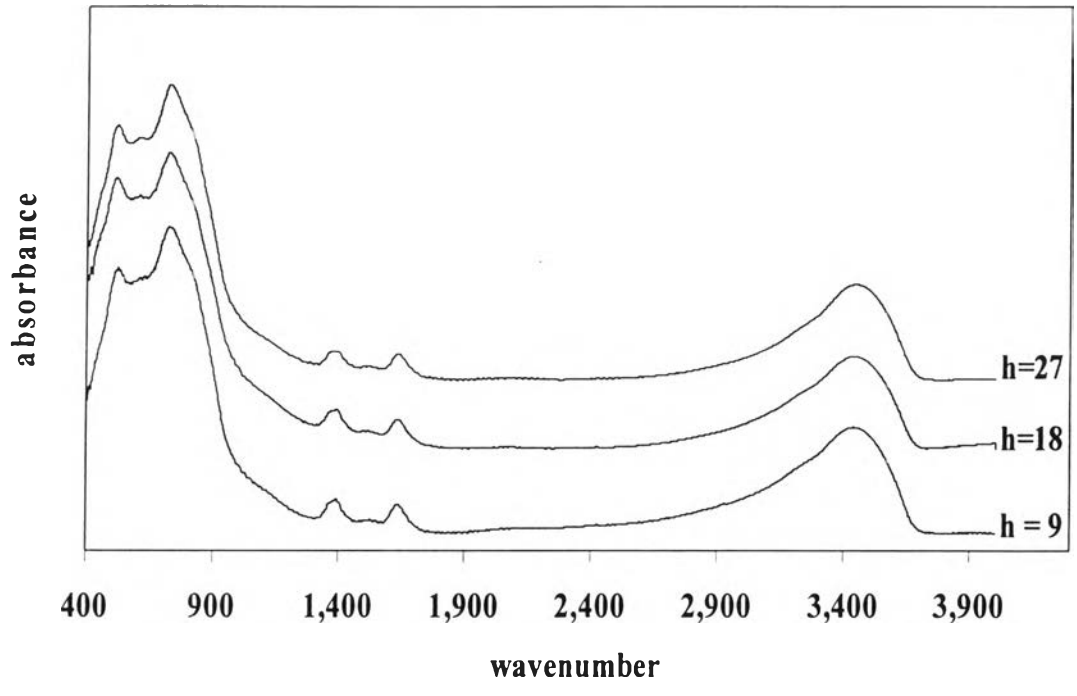
absorbance
h=27
h=18
h = 9
400
900
1,400
1,900
2,400
2,900
3,400
3,900
wavenumber

Figure 11.

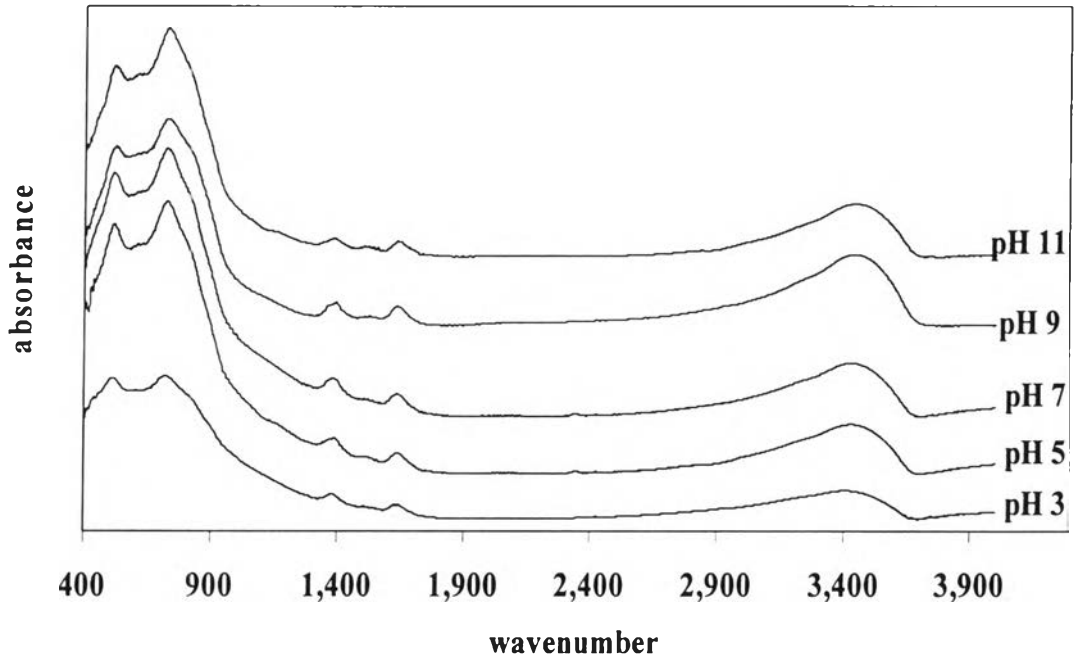
absorbance
pH 11
pH 9
pH 7
pH 5
pH 3
400
900
1,400
1,900
2,400
2,900
3,400
3,900
wavenumber

Figure 12.

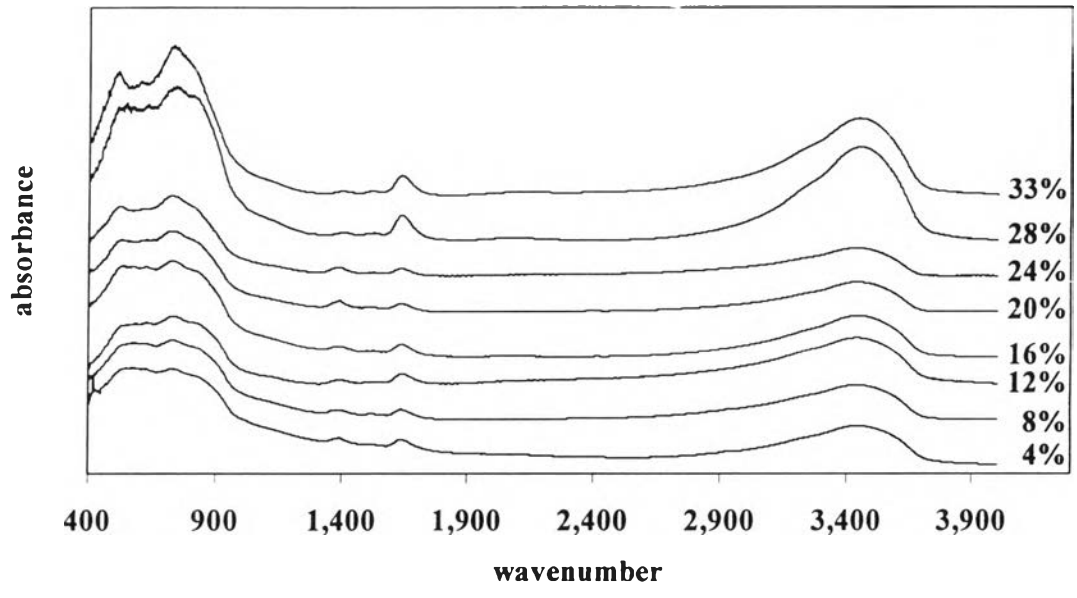
absorbance
33%
28%
24%
20%
16%
12%
8%
4%
400
900
1,400
1,900
2,400
2,900
3,400
3,900
wavenumber

Figure 13.

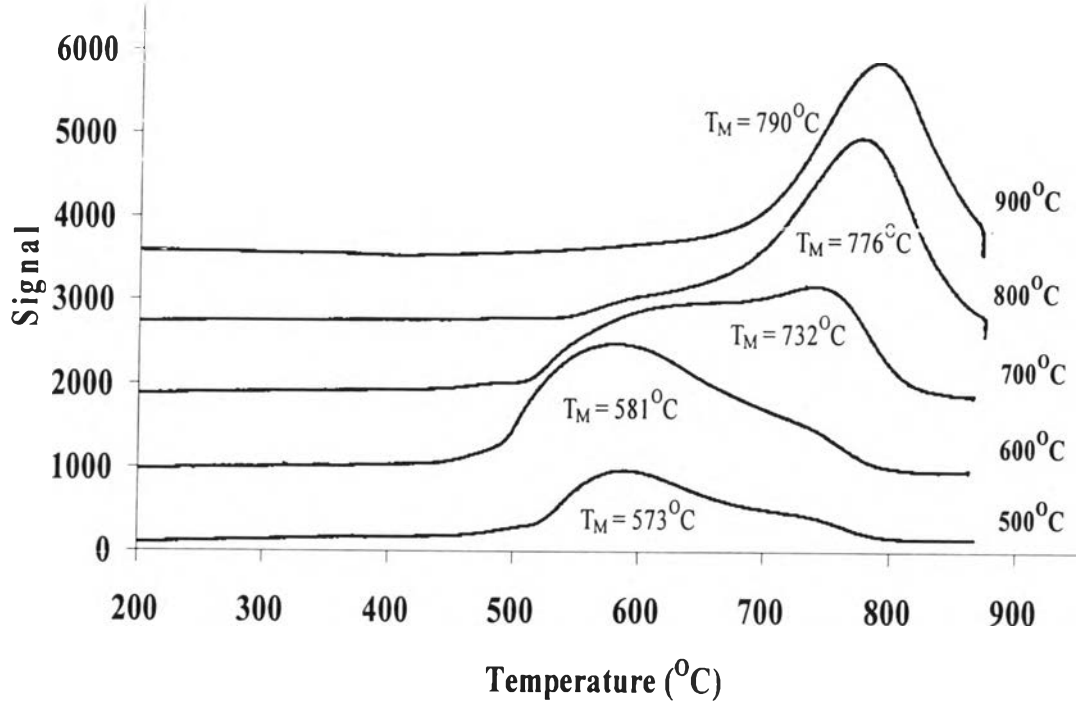
6000
5000
4000
3000
2000
1000
0
Signal
200
300
400
500
600
700
800
900
Temperature (°C)
T_M = 790°C
T_M = 776°C
T_M = 732°C
T_M = 581°C
T_M = 573°C
900°C
800°C
700°C
600°C
500°C

Figure 14.

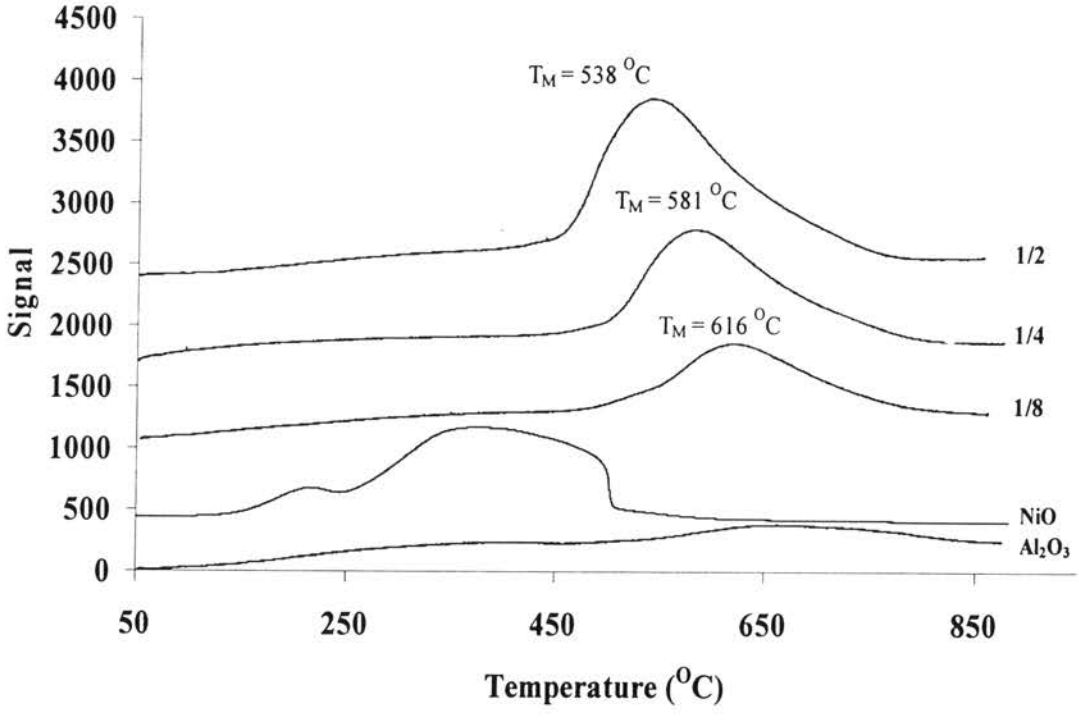
4500
4000
3500
3000
2500
2000
1500
1000
500
0
Signal
$T_M = 538\ ^{O}C$
$T_M = 581\ ^{O}C$
$T_M = 616\ ^{O}C$
1/2
1/4
1/8
NiO
$Al_2O_3$
50
250
450
650
850
Temperature ($^{O}C$)

Figure 15.

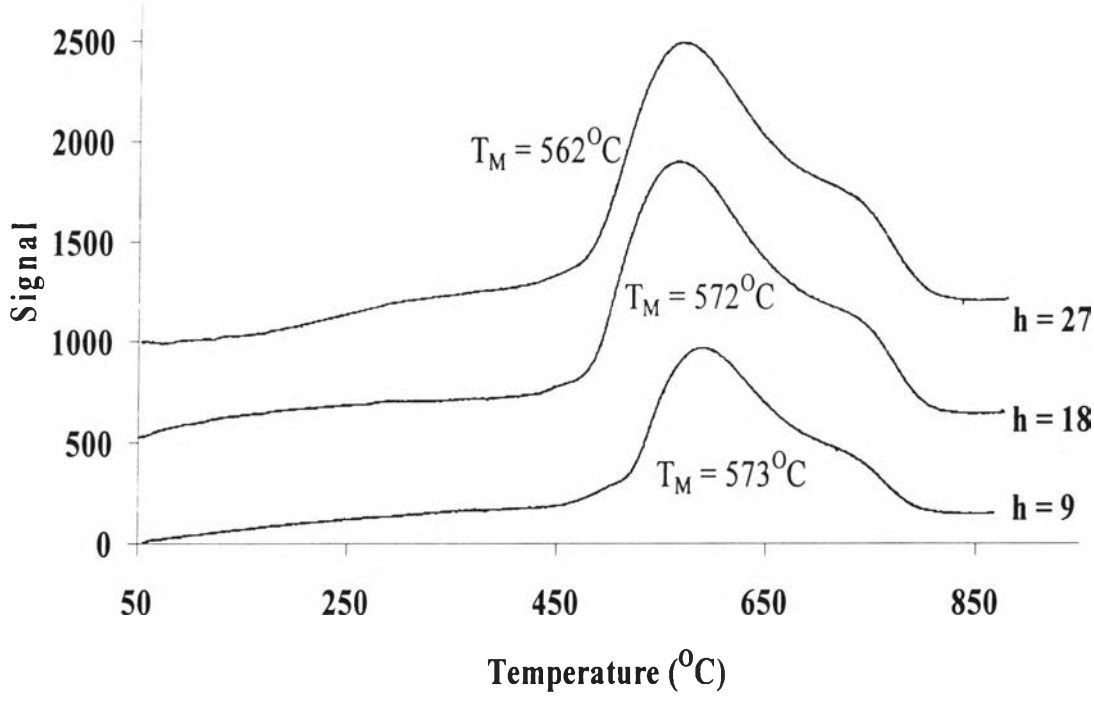
2500
2000
1500
1000
500
0
Signal
$T_M = 562^OC$
$T_M = 572^OC$
$T_M = 573^OC$
h = 27
h = 18
h = 9
50
250
450
650
850
Temperature ($^OC$)

Figure 16.

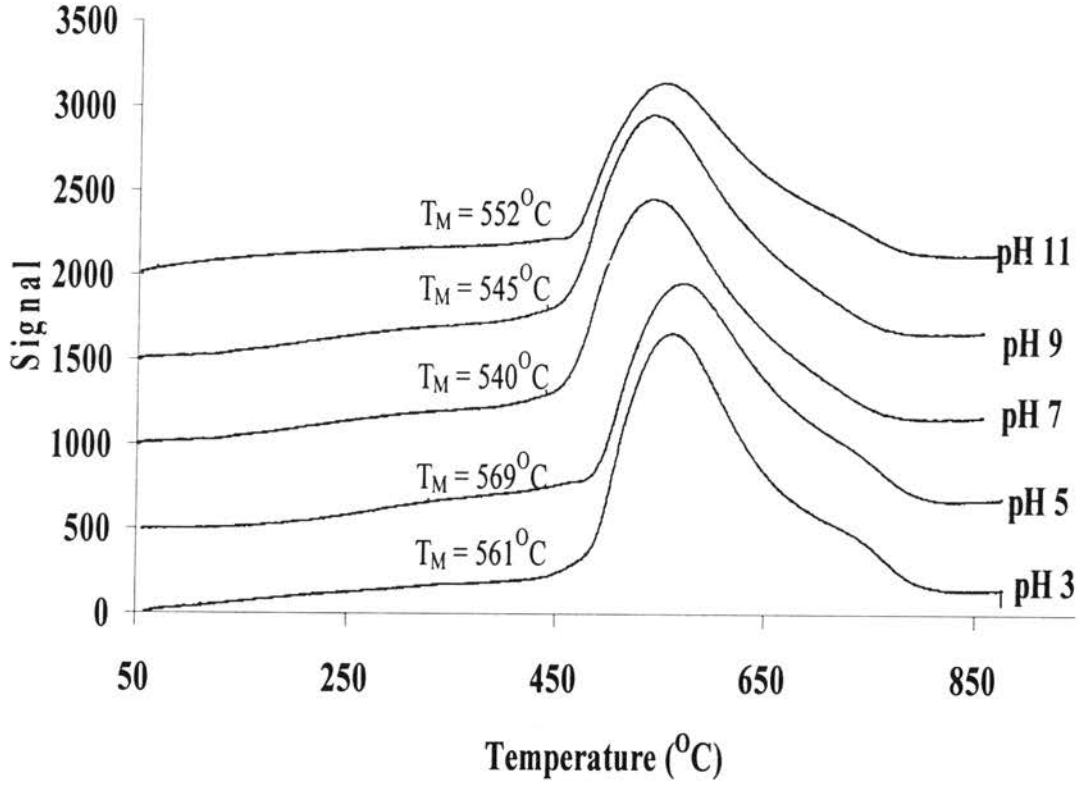
3500
3000
2500
2000
1500
1000
500
0
Signal
50
250
450
650
850
Temperature (°C)
T_M = 552°C
T_M = 545°C
T_M = 540°C
T_M = 569°C
T_M = 561°C
pH 11
pH 9
pH 7
pH 5
pH 3

Figure 17.

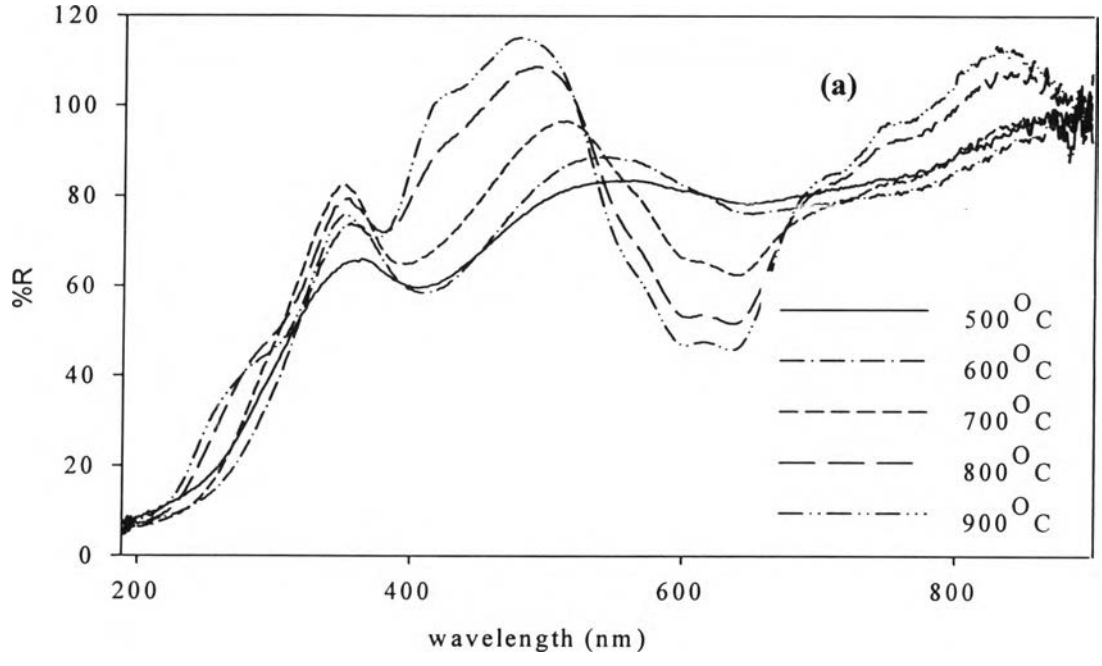
(a)
%R
wavelength (nm)
500 °C
600 °C
700 °C
800 °C
900 °C

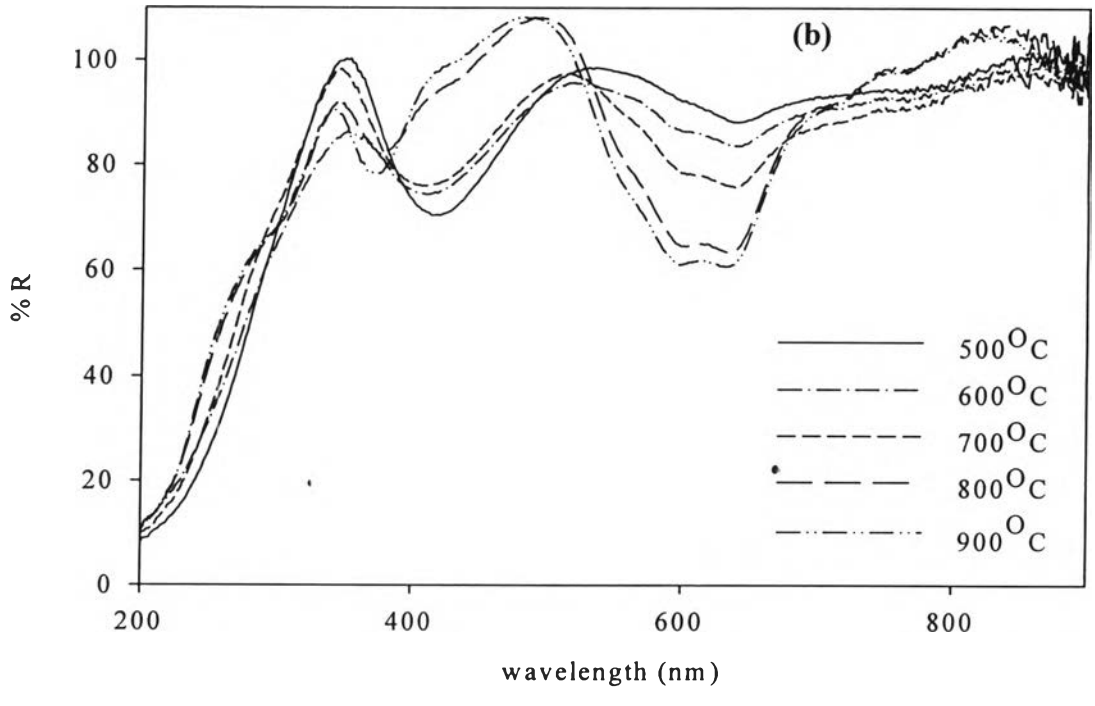
(b)
% R
wavelength (nm)
500°C
600°C
700°C
800°C
900°C

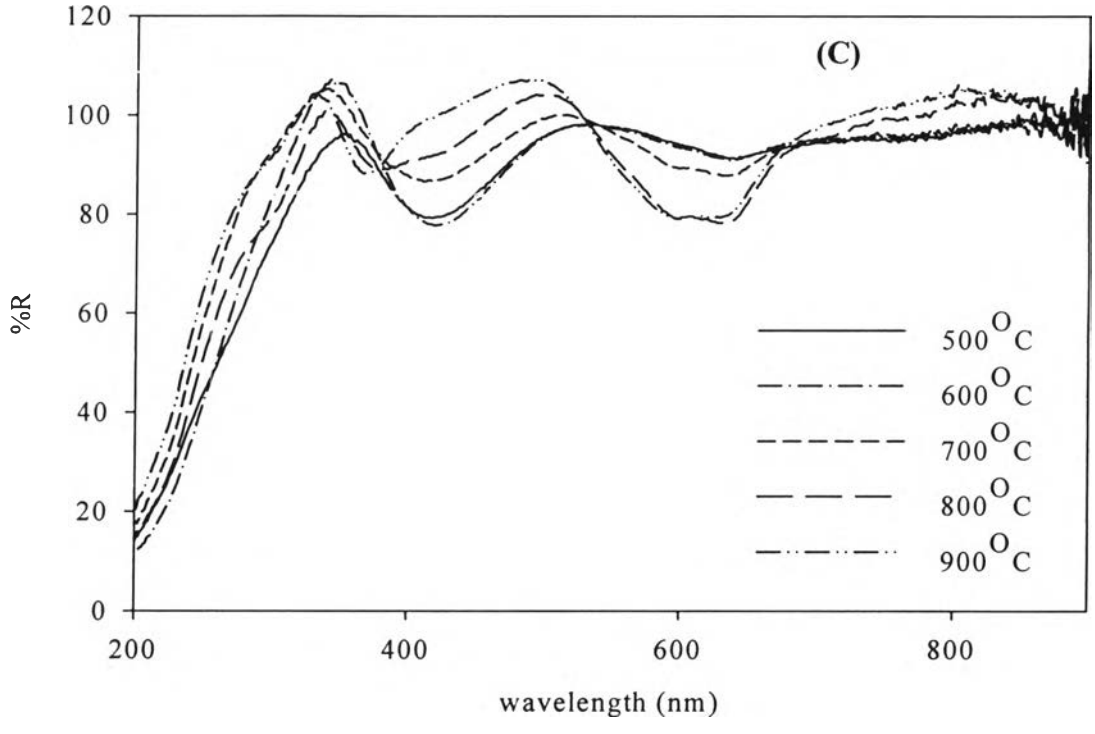
(C)
120
100
80
60
40
20
0
%R
200
400
600
800
wavelength (nm)
500 °C
600 °C
700 °C
800 °C
900 °C

Figure 18.

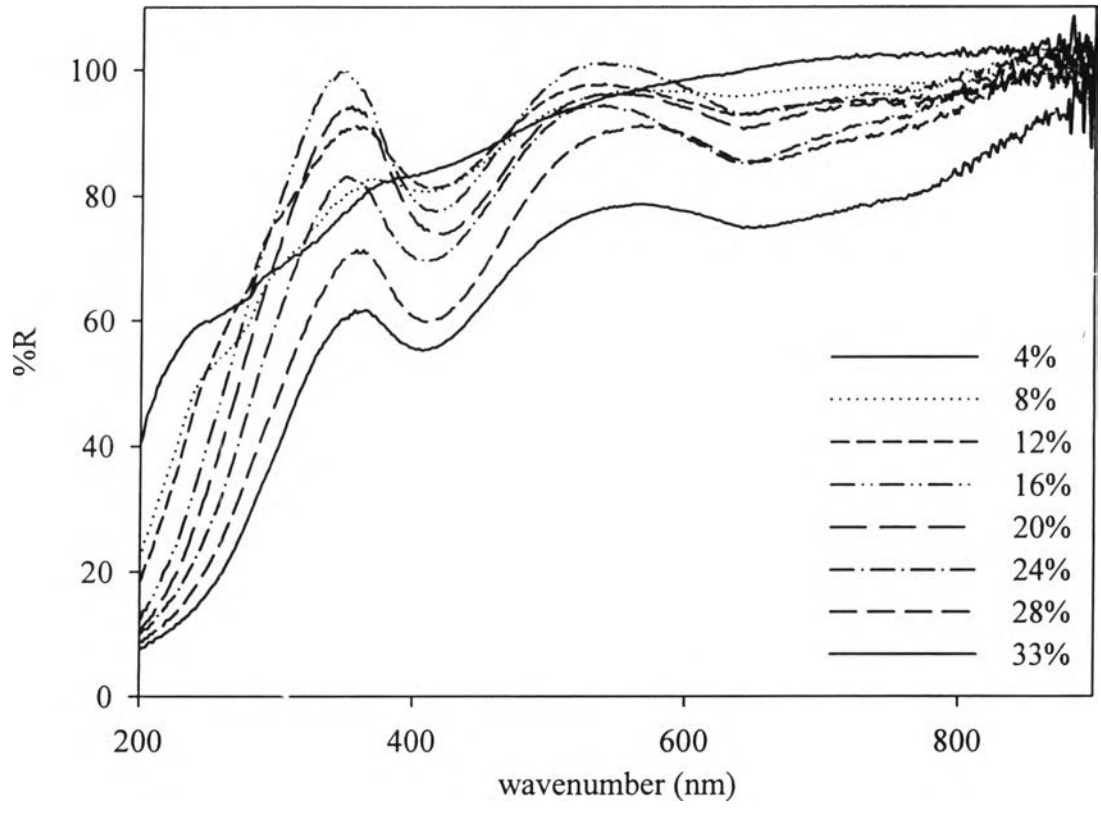
100
80
60
40
20
0
%R
200
400
600
800
wavenumber (nm)
4%
8%
12%
16%
20%
24%
28%
33%

Figure 19.

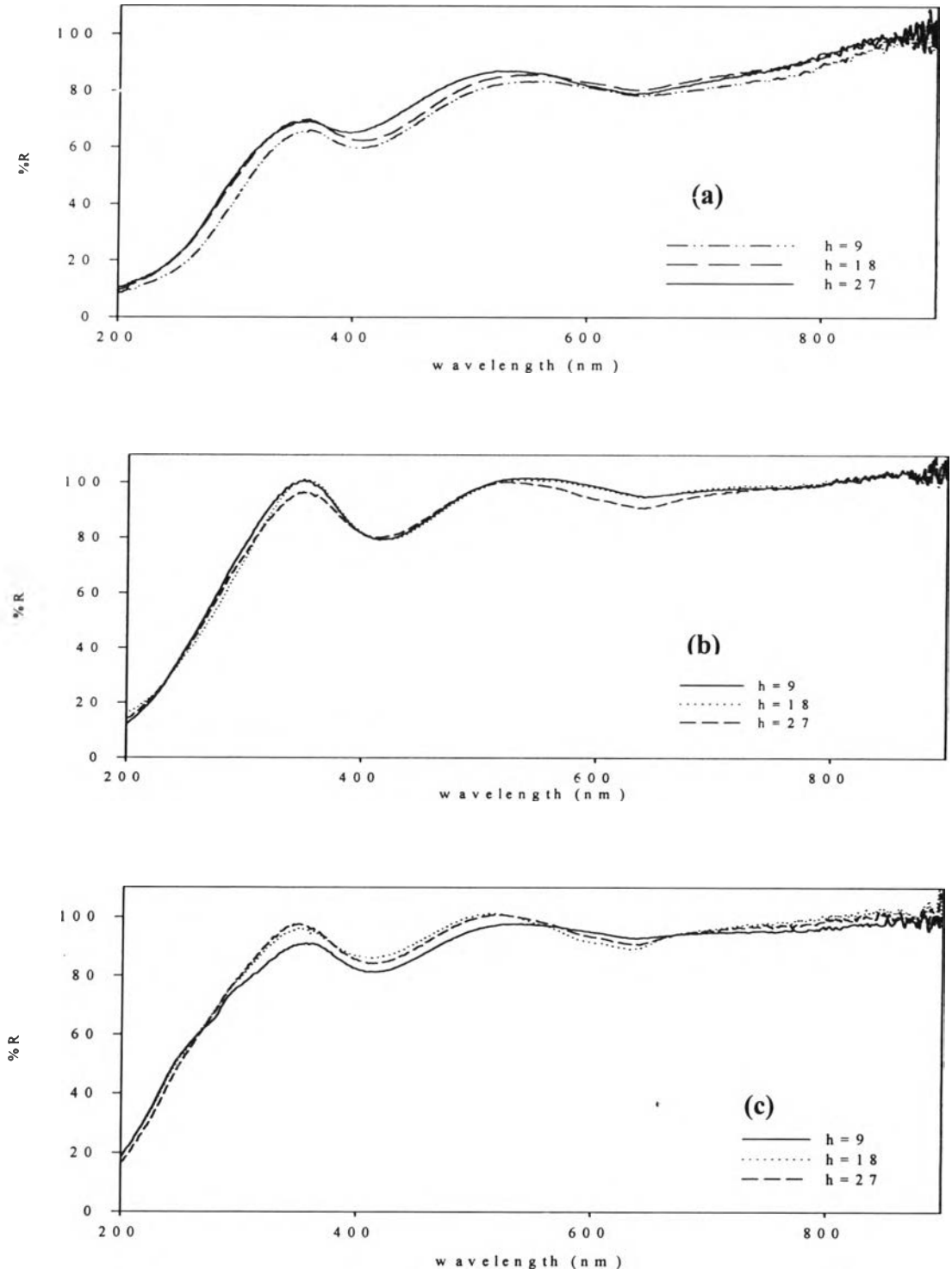
100
80
60
40
20
0
%R
(a)
h = 9
h = 18
h = 27
200
400
600
800
wavelength (nm)
100
80
60
40
20
0
%R
(b)
h = 9
h = 18
h = 27
200
400
600
800
wavelength (nm)
100
80
60
40
20
0
%R
(c)
h = 9
h = 18
h = 27
200
400
600
800
wavelength (nm)

Figure 20.

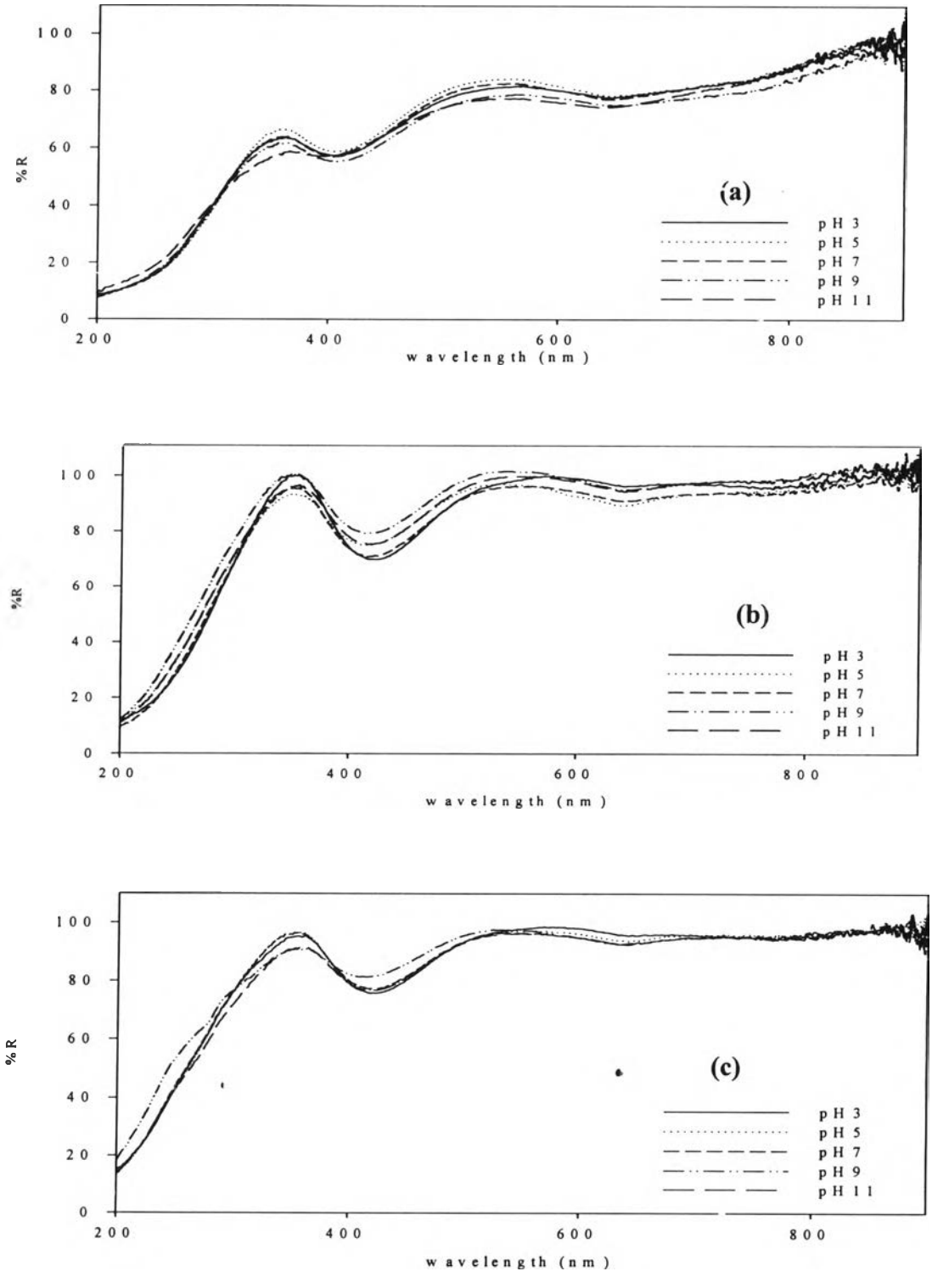
100
80
60
40
20
0
%R
200
400
600
800
wavelength (nm)
(a)
pH 3
pH 5
pH 7
pH 9
pH 11
(b)
(c)

Figure 21.

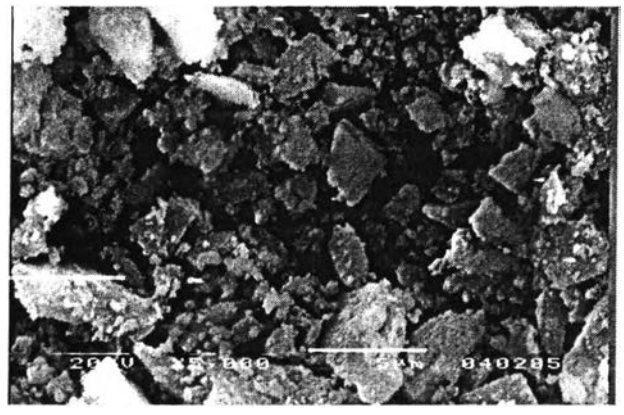

Figure 22 a.

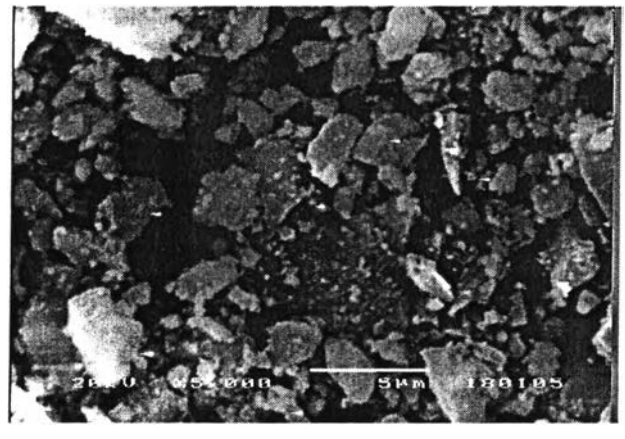

Figure 22 b.

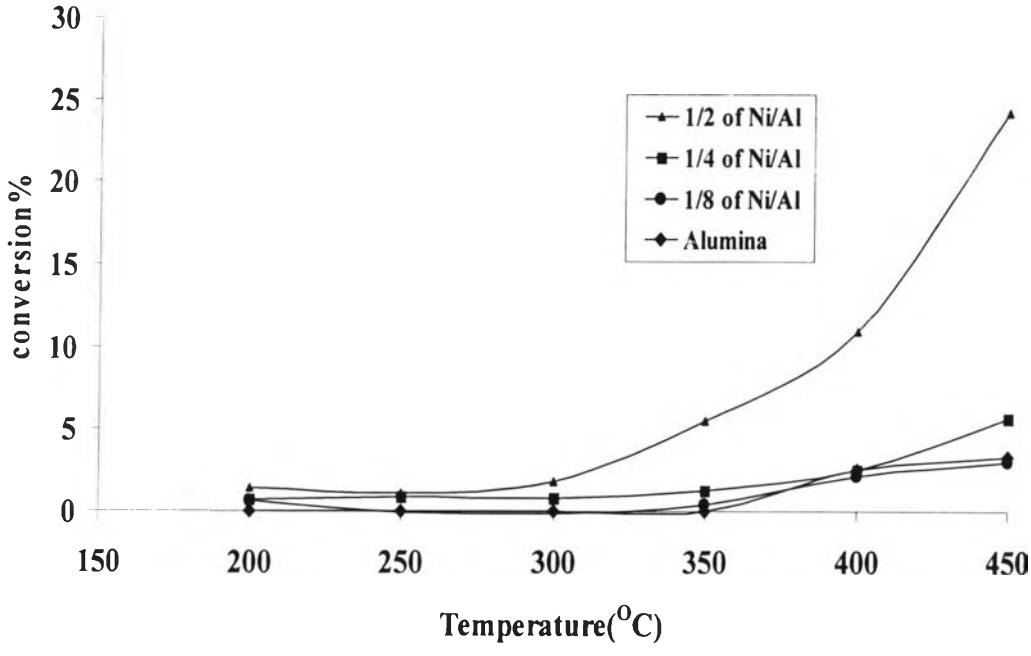
30
25
20
15
10
5
0
conversion%
150
200
250
300
350
400
450
Temperature(°C)
1/2 of Ni/Al
1/4 of Ni/Al
1/8 of Ni/Al
Alumina

Figure 23.

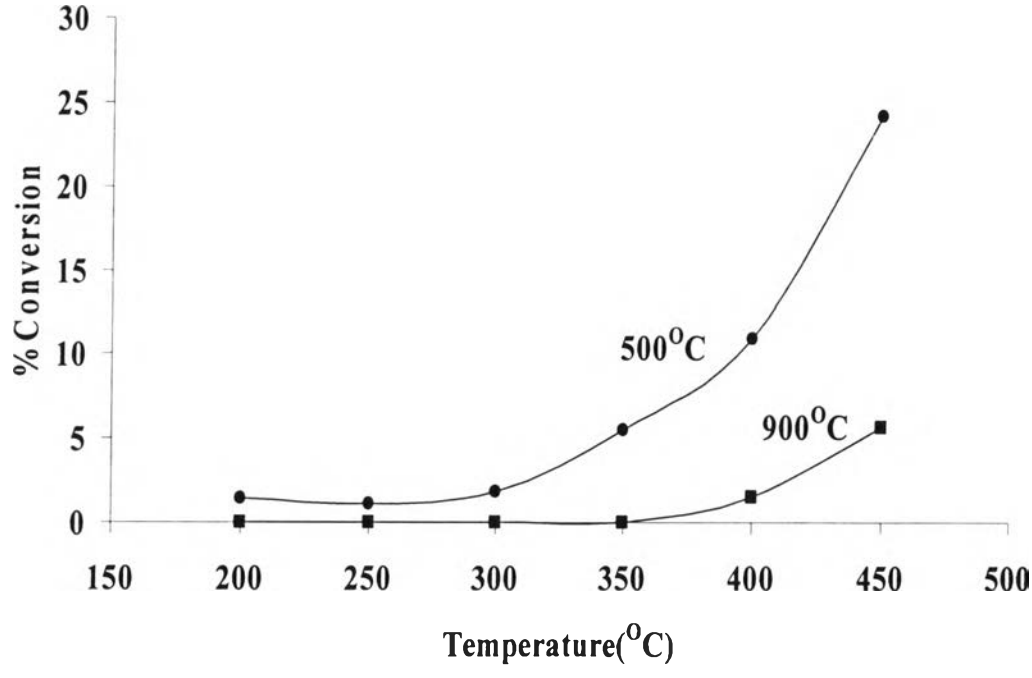
30
25
20
15
10
5
0
% Conversion
500°C
900°C
150
200
250
300
350
400
450
500
Temperature(°C)

Figure 24.

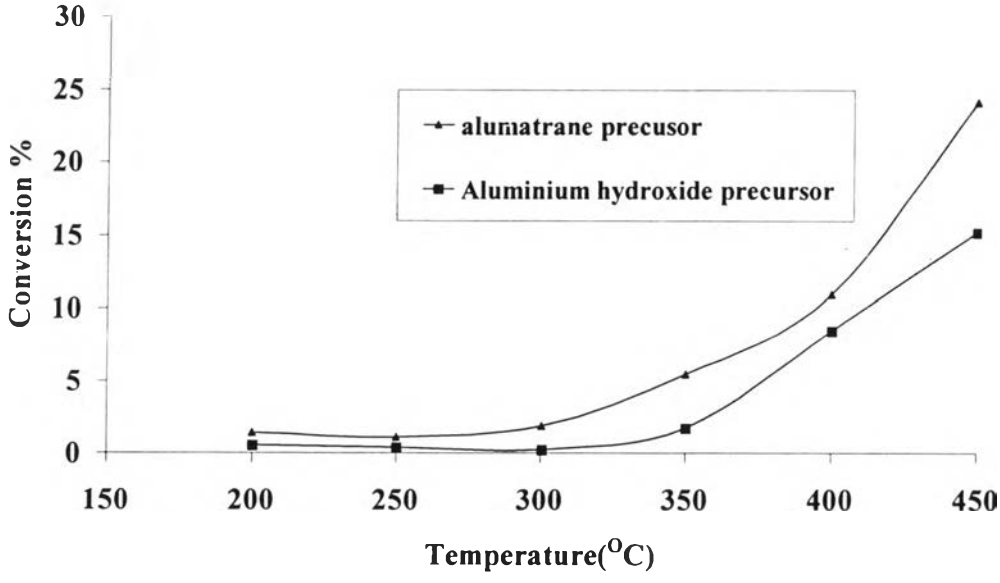
30
25
20
15
10
5
0
Conversion %
alumatrane precusor
Aluminium hydroxide precursor
150
200
250
300
350
400
450
Temperature(OC)

Figure 25.

| Condition | Surface area ($m^2/g$) |
|---|---|
| $Al_2O_3$ | 416 |
| 4% Ni | 416 |
| 8% Ni | 382 |
| 12% Ni | 402 |
| 16% Ni | 380 |
| 20% Ni | 381 |
| 24% Ni | 372 |
| 28% Ni | 405 |
| 33% Ni | 410 |

Table 1.

| Condition | Surface area ($m^2/g$) |
|---|---|
| 1/2 of Ni/Al 500$^{O}$C | 410 |
| 1/2 of Ni/Al 600$^{O}$C | 272 |
| 1/2 of Ni/Al 700$^{O}$C | 260 |
| 1/2 of Ni/Al 800$^{O}$C | 174 |
| 1/2 of Ni/Al 900$^{O}$C | 140 |

Table 2.

| Condition | Surface area ($m^2/g$) of h = 9 | Surface area ($m^2/g$) of h = 18 |
|---|---|---|
| 1/2 of Ni/Al pH 3 | 340 | 337 |
| 1/2 of Ni/Al pH 5 | 360 | 366 |
| 1/2 of Ni/Al pH 7 | 392 | 348 |
| 1/2 of Ni/Al pH 9 | 410 | 422 |
| 1/2 of Ni/Al pH 11 | 380 | 350 |

Table 3.

| Condition | 1/2 of Ni/Al | 1/4 of Ni/Al | 1/8 of Ni/Al |
|---|---|---|---|
| h = 9 | 410 | 381 | 377 |
| h =18 | 422 | 452 | 402 |
| h = 27 | 375 | 416 | 393 |

Table 4.